

# REAL OR INTERLOPER? The Redshift Likelihoods Of $Z > 8$ Galaxies In The Hdf12

Nor Pirzkal<sup>1</sup>, Barry Rothberg<sup>2,3</sup>,  
Russell Ryan<sup>1</sup>, Dan Coe<sup>1</sup>, Sangeeta Malhotra<sup>4</sup>, James Rhoads<sup>4</sup>, AND Kai Noeske<sup>1</sup>

## ABSTRACT

In the absence of spectra, the technique of fitting model galaxy template spectra to observed photometric fluxes has become the workhorse method for determining the redshifts and other properties for high- $z$  galaxy candidates. In this paper, we present an analysis of the most recent and possibly most distant galaxies ( $z \sim 8 - 12$ ) discovered in the Hubble Ultra Deep Field (HUDF) using a more robust method of redshift estimation based on Markov Chain Monte Carlo (MCMC) fitting, in contrast to the “best fit” models obtained using simpler  $\chi^2$  minimization techniques. The advantage of MCMC fitting is the ability to accurately estimate the probability density function of the redshift, for each object as well as any input model parameters. This makes it possible to derive accurate credible intervals by properly marginalizing over all other input model parameters. We apply our method to 13 recently identified sources in the HUDF and show that, despite claims based on  $\chi^2$  minimization, none of these sources can be securely ruled out as low redshift interlopers ( $z < 4$ ) due to the low signal-to-noise of currently available observations. There is an average probability of 21% that these sources are low redshift interlopers.

*Subject headings:* galaxies: high-redshift, galaxies: photometry, galaxies: stellar content, methods: statistical,

---

<sup>1</sup>Space Telescope Science Institute, 3700 San Martin Drive, Baltimore, MD21218, USA

<sup>2</sup>Leibniz-Institut für Astrophysik Potsdam (AIP), An der Sternwarte 16, D-14482, Potsdam, Germany

<sup>3</sup>Department of Physics & Astronomy, George Mason University, MS 3F3, 4400 University Drive, Fairfax, VA 22030, USA

<sup>4</sup>School of Earth And Space Exploration, Arizona State University, Tempe, AZ, 85287-1404, USA

## 1. INTRODUCTION

Over the last 15 yr the ever increasing pace at which new, more sensitive detectors and larger telescope apertures have come online has spurred a fast and furious race to detect the most distant galaxies in the universe. Emission features from HII regions (such as  $\text{Ly}\alpha$ ), have been a useful tool for detecting star-forming galaxies at  $3 < z < 6$  (corresponding to rest-frame optical wavelengths; Malhotra et al. 2001). However, at higher redshifts, corresponding to the first several hundred million years since the big bang, more and more matter was locked up in neutral hydrogen. At these early epochs the neutral intergalactic medium attenuates significant amounts of light from galaxies, including  $\text{Ly}\alpha$ , making detection of these systems more difficult. If  $\text{Ly}\alpha$  is significantly diminished then one must rely on the detection of a continuum break to select candidate galaxies. Detecting galaxies at these redshifts places constraints on the epoch of re-ionization, thought to be at  $z > 6$  (Fan et al. 2006; Komatsu et al. 2011). Detecting and measuring the properties of these galaxies is critical to understand what caused the epoch of re-ionization.

Detecting and measuring the properties of high- $z$  galaxies is not easy. At rest-frame  $\lambda < 1216\text{\AA}$  the flux from high redshift galaxies can be completely vanquished due to the  $\text{Ly}\alpha$  forest absorption and when observed in a filter corresponding to this wavelength the galaxy “drops out.” At  $\lambda > 1216\text{\AA}$  the flux is not attenuated and can be detected. Such breaks become more pronounced with redshift, for example at  $z > 5.7$  a break corresponds to  $\sim 3.4$  mag in color (e.g. Songaila & Cowie 2002; Hu et al. 2004). Detection at  $z > 8$  is further complicated by the fact that the Lyman regime is redshifted into near-infrared wavelengths ( $\lambda > 1\text{ }\mu\text{m}$ ) where bright atmospheric telluric skylines and strong telluric absorption features force ground-based observations to use specific and restrictive atmospheric windows. *Large Hubble Space Telescope (HST)* based spectroscopic surveys such as GRAPES and PEARS (Pirzkal et al. 2004) have demonstrated the power of low resolution spectroscopy to identify high redshift sources (Malhotra et al. 2005; Rhoads et al. 2009). However, until similar large-scale programs are implemented in the near-IR using the WFC3/*HST* or *James Webb Space Telescope (JWST)*, the next best method for detecting the most distant galaxies relies on using near-IR photometry obtained with *HST*.

Recently, the race to find the earliest galaxies has relied more and more on the use of the near-infrared Wide Field Camera 3 (WFC3) detector ( $1 < \lambda < 1.6\text{ }\mu\text{m}$ ) on the *HST*, and in particular, broad-band imaging. Detecting possible  $1216\text{\AA}$  breaks with *HST* photometry should be straightforward, assuming one collects a sufficient amount of photons. However, observations must first contend with the possibility of foreground interlopers. At  $z \sim 6$  foreground interlopers can be as frequent as 45% for observations with signal-to-noise  $(\text{S/N}) < 5$  (e.g. Dickinson et al. 2004; Stanway et al. 2008). Without the direct detection of spectroscopic lines, redshift confirmations must rely on Spectral Energy Distribution (SED)

fitting.

One of the first tools used to derive photometric redshifts was the SED fitting code **hyperz** which simply maximizes the likelihood by brute-force using a grid of SED templates (Bolzonella et al. 2000). As noted in Bolzonella et al. (2000): “Both the  $z_{\text{phot}}$  and the SED are obtained through **hyperz**, together with the best fit parameters ( $A_V$ , spectral type, metallicity and age). Because of the degeneracy between these parameters, the relevant information shall be the redshift and the rough SED type, in the sense that a given object has a “blue” or “red” continuum at a given  $z$ , but no reliable information can be obtained about the other parameters from broad-band photometry alone.” Despite this, **hyperz** and other similar  $\chi^2$  minimization SED fitting codes (e.g. Thompson et al. 2001; Papovich et al. 2001; Labbé et al. 2003; Schaerer & Pelló 2005; Mobasher et al. 2005; Pirzkal et al. 2007; McLure et al. 2009) have been used to extract more than just redshifts, including these degenerate properties. All of which is based on simply selecting the template with the smallest  $\chi^2$ .

This has led to a number of situations in which photometric redshifts and galaxy properties determined from  $\chi^2$  minimization SED fitting have produced questionable claims of high- $z$  galaxies. Pelló et al. (2004) claimed the discovery of a  $z = 10$  galaxy from a combination of deep  $J$ ,  $H$ ,  $K$  photometry obtained from the *Very Large Telescope (VLT)*, *HST* optical imaging, and  $J$ -band spectroscopy from ISAAC/VLT. While Pelló et al. (2004) claimed a detection of Ly $\alpha$  from low S/N ISAAC/VLT spectra, the basis for the claim relied primarily on SED fitting using a modified form of **hyperz** with stacked  $J$ ,  $H$ ,  $K$  imaging. Followup deep  $V$ -band ( $V_{\text{AB}} = 27.8$  mag) imaging from the VLT (Lehnert et al. 2005) and deeper  $H$ -band imaging from Gemini/NIRI (Bremer et al. 2004) failed to detect fluxes predicted from the SED fitting. These imaging results and a re-analysis of the spectra by Weatherley, et al. (2004) led to the conclusion that the object was a spurious detection, even though the fits from **hyperz** produced an excellent  $\chi^2$  fit. Mobasher et al. (2005) claimed the detection of a strong Balmer break between  $H$ -band and the *Spitzer* IRAC1 ( $3.6 \mu\text{m}$ ) bands. Simply selecting the best-fit reduced  $\chi^2$  model led the authors to conclude that the object was a massive early-type galaxy  $z = 6.5$ , a stark contrast to the types of systems that should exist at this epoch. Their results raised serious questions regarding the viability of the  $\Lambda$ -CDM paradigm of building bigger galaxies from smaller building blocks. The next best-fit model, from a secondary  $\chi^2$  minimum, was a “dusty” starburst at  $z \sim 2.5$  with  $E(B - V) = 0.7$ . This model was rejected because it was considered too dusty at this redshift to be physically real, even though the authors estimated the probability of this fit to be 15%. Revised SED-fitting, using newer 16 and  $22 \mu\text{m}$  photometry obtained with the IRS instrument on *Spitzer*, produced a best-fit for a  $z = 1.7$  luminous infrared galaxy with a significant ( $A_V \sim 3 - 4$ ) amount of dust (Chary et al. 2007). Similarly, Henry et al. (2008) claimed the discovery of a Lyman break galaxy at  $z \sim 9$  from NICMOS/*HST* imaging (based on a  $F110W$  dropout) and *Spitzer* imaging. Their  $\chi^2$  minimization fitting rejected local minima models at  $z \sim 2 -$

3 (produced by the degeneracy among the parameters). Subsequently, it was observations from MMT/Megacam blueward of the claimed break ( $i' = 26$  mag) that demonstrated the intermediate redshift solutions that were initially rejected were actually correct (Henry et al. 2009). Finally, Capak et al. (2011) presented three  $z$ -band dropout candidates in which  $\chi^2$  minimization fitting produced best solutions at  $z > 7$ , only to find that followup imaging of one blueward of the claimed break and at  $24 \mu\text{m}$  better supported at  $z \sim 1.7$  solution; and a second with observed  $H$ -band flux (from NIRSPEC/Keck spectroscopy) weaker than predicted by SED models.

The authors of the works described above did not imply that low redshift solutions were entirely excluded, but selected high- $z$  solutions based primarily on the  $\chi^2$ . Determining the accurate probability of these objects being at low redshift is therefore important.

Any SED fitting effort is further complicated by the assumption that model galaxy spectra constructed from our knowledge of how stars evolve in the local universe is equally applicable to the earliest epochs. One should also be cognizant of the fact that the rest-frame wavelength range sampled by a fixed set of photometric filters will span a narrower range with increasing redshift. For the most recent claims of galaxies at  $8 < z < 12$  (e.g. Yan et al. 2010; Bouwens et al. 2011; Ellis et al. 2013), WFC3/IR covers only  $\Delta\lambda \sim 560$  and  $390 \text{ \AA}$ , (for  $z = 8$  and  $z = 12$ , respectively, and excluding the  $1216\text{\AA}$  break itself). Including the less sensitive and lower resolution IRAC1 and IRAC2 channels only widens this to  $\Delta\lambda \sim 3700$  and  $2600 \text{ \AA}$  for  $z = 8$  and  $12$ , respectively. Strong statistical priors exist for only a handful of lensed galaxies (e.g. Coe et al. 2013). Recent work from Atek et al. (2011) furthermore shows that there exists a population of low redshift galaxies with strong emission lines that can mimic the color-selection criteria used to select  $z \sim 8$  galaxies. The relative lack of information about high redshift galaxy candidates, as well as the low S/N of the observations produce a situation where using sound statistical methods is particularly important when trying to determine the redshifts of these objects.

The latest claims of  $z > 8$  galaxies based on  $\chi^2$  minimization SED fitting have been presented by Bouwens et al. (2011), Yan et al. (2010), and Ellis et al. (2013) using deep WFC3/IR images of the Hubble Ultra Deep Field (HUDF). The results from Ellis et al. (2013) are particularly interesting since this project adds additional data (GO 12498; PI: Ellis, HUDF12) to the HUDF09 field (GO 11563; PI: Illingworth) in the F105W and F160W filters as well as new observations with the F140W filter. This filter spans a wavelength range inaccessible from the ground. All but one of the sources listed in Bouwens et al. (2011) and none of the sources listed in Yan et al. (2010) were confirmed to be at  $z > 8.5$  using these new deeper data.

The new near-infrared measurements from the HUDF12 are the deepest observations

available to date and for the foreseeable future. When combined with ancillary data from the HDUF09, these data allow one to construct spectral energy distributions of these sources spanning from observed  $B$ -band (ACS  $F435W$ ) to IRAC1 and IRAC2 channels (3.4 and 4.6  $\mu\text{m}$ , respectively). The 13 objects listed in Ellis et al. (2013) show large red colors consistent with strong spectral breaks. While followup spectroscopic observations have only been attempted on one of the targets, UDFy-38135539 (Lehnert et al. 2010; Bunker et al. 2013) and will be discussed later, the objects have all been fit using what is now considered the “standard method” of minimized  $\chi^2$  SED fitting, yielding redshifts of  $8 < z < 12$ . Given the limitations of this method, and the numerous examples of what later turned out to be incorrect redshift identifications, we are motivated to apply more robust Bayesian techniques to better constrain the physical parameters of galaxies observed using broad band filters. Central to this effort is the need to derive realistic estimates of the uncertainties for each derived parameter.

Thus, using the sources and fluxes, including Advanced Camera for Surveys (ACS), WFC3 and IRAC, provided in Ellis et al. (2013), and reference therein, for 13 candidate high- $z$  1216Å break galaxies we employ  $\pi\text{MC}^2$ , a Markov Chain Monte Carlo (MCMC) approach (for details see Pirzkal et al. 2012a,b). For the purpose of this paper we define low redshift to be  $z < 4$  and high redshift to be  $z > 4$ . Further, we treat equally all 13 objects listed in Ellis et al. (2013) as potential high redshift candidates to be tested with  $\pi\text{MC}^2$ . We are not implying that  $\pi\text{MC}^2$  is the only viable method to perform this type of analysis. MCMC is a well established approach to this type of problem. The marginal S/N of current high redshift candidates observations warrant more robust techniques than the common  $\chi^2$  minimization technique and the reliance on a single “best fit” model provided by **hyper**-derived SED fitting software.

## 2. APPLIED TECHNIQUES: MINIMIZED $\chi^2$ SED FITTING VERSUS $\pi\text{MC}^2$

Nominally, the “standard method” of minimized  $\chi^2$  SED fitting works by matching photometric fluxes to a pre-selected grid of model templates until the residuals between model and data are minimized. However, the choice of input models, the number of parameters (and whether any are constrained), parameter degeneracy and if the models sufficiently sample the entire range of the physical parameter space all affect the outcome of the fit. Any and all of these issues can produce “best-fit” solutions that are unphysical (i.e. a very old object in a young universe as in Labbé et al. (2010) and Richard et al. (2011)). Once the number of model parameters to be fit exceeds three it becomes computationally inefficient to

fit parameter grid SEDs, more so for errors because each parameter must be refit following a pure Monte Carlo approach (e.g. each parameter requires several thousand additional iterations). All of the most recent *HST* based high- $z$  candidate objects have relied on some modified implementation of the **hyperz** photometric code, or similar  $\chi^2$  SED minimization techniques (e.g. McLure et al. 2010, 2011; Bouwens et al. 2011; Ellis et al. 2013). While **hyperz** has proven to be capable for accurately constraining low- $z$  photometric redshifts for large numbers of sources in deep, often crowded fields later confirmed with spectroscopic followup, it was designed to estimate the *most likely* photometric redshift, not produce credible intervals. Its treatment of the probability density functions (PDFs) is inadequate. Based on the **hyperz** Users Manual and J.-M. Miralles (2013, private communication) it minimizes over the extra dimensions ( $\mathbf{T}$ ) instead of marginalizing over them, therefore the PDF returned by **hyperz** is given by:

$$p_{\text{hyperz}}(z) = \min_{\mathbf{T}} p(z, \mathbf{T}) \quad (1)$$

This approach does not account for the *volume* of the parameter space probed resulting in unreliable confidence intervals, particularly in the case of additional maxima. While such a distribution may be somewhat useful, the credible intervals produced by **hyperz** should not be trusted (J.-M. Miralles 2013, private communication).

In contrast, MCMC, and our implementation of it,  $\pi\text{MC}^2$ , is a method which randomly samples the entire parameter space but does not probe the multidimensional region uniformly. The posterior probability distribution function can be constructed by simply creating a histogram of the values of a given parameter in the MCMC chain from values taken after it converges (see Section 2 in Pirzkal et al. 2012a, for more details). Just as in Pirzkal et al. (2012a) we quote both the 95% and 68% credible regions here (see Section 2.1 of Pirzkal et al. (2012a) for a discussion of 95% versus 68% credible regions, which we take to be the 95% and 68% highest posterior density, or HPD, regions, respectively). While computationally more expensive (yet more efficient), our current implementation of the MCMC SED fitting code,  $\pi\text{MC}^2$ , has three main features:

1. It does not depend on a pre-defined input model parameter grid and allows for a computationally efficient exploration of the input parameter space.
2. the effect of nebular emission lines and nebular emission continuum can be included.
3. It allows one to derive a statistically valid posterior PDF for each of the input parameters by integrating over the remaining parameters:

$$p(z) = \int p(z, \mathbf{T}) d\mathbf{T} \quad (2)$$

To properly assess the possibility of lower-redshift solutions, it is imperative that the volume of parameter space be taken into account by integrating over the additional degrees of

freedom.

We have applied  $\pi\text{MC}^2$  to the sample of high redshift candidates listed in Ellis et al. (2013) because this sample is based on the deepest *HST* observations to date and provides candidate objects that could be the faintest examples of Lyman break galaxies. Here, the analysis of redshifts and other parameters using the photometric fluxes from Ellis et al. (2013) are based upon using the use of stellar population models from Bruzual & Charlot (2003, BC03), Charlot and Bruzual (2013, CB07), and Maraston (2005, MA05) in conjunction with  $\pi\text{MC}^2$ . The parameters investigated include: stellar mass; a broad range of extinction values ( $0 < A_V < 10$ ); metallicity ( $0.005 < Z < 0.05$ ); and stellar population ages (limited only by the age of the universe at a given redshift). We adopted flat priors for these parameters. We choose flat priors as these most closely match those used by Ellis et al. (2013), but we allowed for larger values of extinction. Using a flat prior for the redshift is a conservative choice because it does not predispose the likelihood towards low or high redshifts. A redshift prior heavily biased towards higher redshift would further reduce the likelihood of these sources to be low redshift interlopers. The application of these models has also been tested with and without the effects of nebular continuum and emission lines (as parameterized by the escape fraction parameter). Details regarding the application of continuum nebular emission and emission lines to  $\pi\text{MC}^2$  can be found in Section 2.2 of Pirzkal et al. (2012a). In addition to using single stellar population models (SSP), the BC03 models were also tested using an exponentially decaying star formation history (SFH) model (parameterized by  $\tau$ ). We use these stellar populations because we are confident that  $\pi\text{MC}^2$  handles them properly and we have extensively tested them. They also match the stellar population models used by Ellis et al. (2013) and we would like to be able to compare the results of applying an MCMC approach without increasing the complexity of the comparison with previous results. We note that some (e.g., Papovich et al. 2011) have advocated the use of a rising exponential star formation rate which would be useful to include in future analyses of these objects. Thus, there are seven discrete population models used with  $\pi\text{MC}^2$ :

- (1) AaSSP BC03 model with nebular contribution;
- (2) a SSP BC03 model without nebular contribution;
- (3) a BC03 model with  $e^{-t/\tau}$  star-formation history and without nebular contribution;
- (4) a SSP CB07 model with nebular contribution;
- (5) a SSP CB07 model without nebular contribution;
- (6) a SSP M05 model with nebular contribution; and
- (7) a SSP M05 model without nebular contribution.

### 3. RESULTS

#### 3.1. Redshift Constraints

A subset of the stellar population parameters, obtained using  $\pi\text{MC}^2$  and BC03 stellar population model with nebular emission, is presented in the first five columns of Table 3. For the most part, the redshift, extinction, stellar ages, stellar masses and metallicity ranges are uniform among the seven input models we used with  $\pi\text{MC}^2$ . Any particular outliers are noted in Table 1.

The results using the BC03 are representative of what is derived for nearly all of the models. Table 3 lists the 68% and the 95% credible intervals derived using  $\pi\text{MC}^2$ . Table 1 clearly shows that the 95% credible regions do *not* strongly constrain the redshift ranges of most of the sources. It is also clear from Table 1 that the 95% credible intervals are much larger than the 68% credible intervals which means that redshift posterior PDFs are *not* Gaussian.

A comparison of the quality of the fits (parameterized as the log likelihood computed by MCMC) from the most representative high redshift ( $z > 4$ ) solution and that of the most representative low redshift ( $z < 4$ ) solution, shows that high redshift models *appear* to fit the observations better than lower redshift models. As a first step, we can examine whether high redshift models always fit the data *significantly* better than alternative low redshift models by computing the significance  $p$  of a likelihood ratio test. This is a comparison between the log likelihood of the best fitting (usually  $z > 4$ ) and best fitting low- $z$  ( $z < 4$ ) models. If  $p > 0.05$  then the hypothesis that the high- $z$  model fits the observation better than the low- $z$  model is rejected at the  $2\sigma$  level.

While we used stellar population models both with and without the effect of nebular lines, we find that when using BC03 models without nebular emission, 7 of the 13 sources are reasonably fit by low redshift models. However, if nebular emission is included then *12 out of 13* objects are reasonably fit (i.e.  $p > 0.05$ ) by low redshift models. The full range of  $p$  values obtained from using different stellar population models are shown in Table 3. Clearly, the quality of the fits is not enough to confidently rule out these sources as low redshift interlopers.

The MCMC methodology also allows us to compute the *actual* probability that a source is at  $z < 4$ ,  $P(z < 4)$ , by integrating the posterior PDF of each object. The range of  $P(z < 4)$  values across all seven stellar population models described above is shown in the last column of Table 3. Low redshift solutions *cannot* be strongly excluded based on the observed photometric break for many of the objects listed in Table 3. When examining the results using all seven stellar population models, 9 out of 13 objects cannot be ruled out (i.e.  $P(z < 4) > 0.05$ ) as low redshift interlopers in the best case scenario (i.e. selecting the



stellar population models that most favor high redshift solutions), and none out of 13 in the worst case scenario (i.e. selecting the stellar population models that most favor low redshift solutions).

Low redshift ( $z < 4$ ) solutions can, at best, be excluded at the  $2\sigma$  confidence level ( $P(z < 4) < 0.05$ ) for only four sources (UDF12-3947-8076, UDF12-3954-6284, UDFy-3779600 and UDFy-38135539). For each of the seven stellar population, the average probability for  $P(z < 4)$ , averaged across all 13 sources, is remarkably consistent and ranges from 19% to 26% with a global average of 21%. We conclude that  $\approx 21\%$  of the sources in Table 3 are therefore likely to be low redshift interlopers.

As in the case of earlier attempts to detect high- $z$  systems (e.g. Henry et al. 2009), it turns out that the limiting sensitivities of fluxes *blueward* of the presumptive break (i.e. ACS bands in our case) are not sufficient to provide strong constraints for the redshifts proposed by simple minimized  $\chi^2$  and "best fit" model SED fitting. Similarly, the IRAC observations are too shallow to provide enough constraints on the rest frame optical light from most of these objects.

In the case of four sources for which low- $z$  solutions can be *statistically* rejected, three (UDF12-3947-8076, UDFy-3779600 and UDFy-38135539) are y-band dropouts and the brightest objects in the sample. Thus, relative to the ACS and IRAC detection limits, they have enough flux in the WFC3 bands to produce a change in flux strong enough to resemble a  $1216\text{\AA}$  decrement. The third object, UDF12-3954-6284, is very faint and only detected in *one* band. By definition it is a marginally acceptable candidate because it is only detected in one band (as noted by Ellis et al. 2013). It is possible that the observed photometric break could be caused by a strong emission line at low- $z$  (see Section 4).

The ACS and IRAC detection limits are too high to unambiguously identify a  $1216\text{\AA}$  decrement for the remaining nine objects in the sample. We estimate that the ACS and IRAC detection limits are  $\approx 5$  and  $\approx 3$  times too high (respectively) to distinguish between a  $1216\text{\AA}$  decrement and a Balmer break in sources this faint. This remains the main limiting factor in securely identifying sources at  $z > 8.5$  using WFC3 observations of the HUDF.

In Figure 1 we show the SEDs of objects UDF12-3954-6284 and UDFy-37796000. The first example is meant to illustrate how too high of rest frame optical limits do not allow to reject low redshift solutions. The second example shows a clear detection of a strong photometric break as well as constraining limits in both the rest frame UV and optical bands. In the case of UDF12-3954-6284, the IRAC detection limits are clearly too high to rule out that this object is a low redshift interloper, if we allow for nebular emission. The log likelihood of the high- $z$  and low- $z$  solutions for this object are 720.9 and 722.4 with a likelihood ratio test confidence of 0.08 which indicates that the high redshift model does not fit the observation significantly (i.e.  $2\sigma$ ) better than the low redshift model. While models lacking nebular emission clearly favor a high redshift solution for this object, the break can clearly

be reproduced by an emission line.

A low redshift solution is much less likely in the case of the significantly brighter object UDFy-37796000 with a redshift of  $\approx 1.6$  and  $A_V = 2.8$ . The log likelihoods of the high and low redshift solutions are 722.6 and 717.5, respectively, resulting in a very low likelihood ratio test confidence values. This case demonstrates how strong rest-frame near UV and optical limits can help rule out a Balmer break.

### 3.2. Secondary Parameters

In addition to redshift constraints  $\pi\text{MC}^2$  was used to determine other parameters including: stellar population ages; extinction; metallicity; and stellar mass. In the cases where models included nebular continuum, the escape fractions were determined; and in the case of BC03 with an exponentially decaying starburst, value of  $\tau$  were derived. The 95% and 68% credible regions estimates for these parameters are given in Table 3 for each object. In the cases of three parameters: metallicity, escape fraction, and  $\tau$  the posterior PDFs were essentially flat. This confirms results from Pirzkal et al. (2012a) where it was demonstrated that these parameters can only be constrained using very high precision photometry (i.e. better than 1% level when using broad-band photometry), which is not the case for the HUDF12, and that simply increasing the number of broad-band filter observations is not sufficient.

The interdependence of the input model parameters is illustrated in Figure 2 which shows the two dimensional distribution of the posterior PDF's for UDF12-3895-7114. The statistically more likely regions are shown using proportionally lighter shades. This figure illustrates the statistical complexity of fitting high redshift sources to stellar population models, the non Gaussian nature of many of the input model parameter PDF's, as well as the low redshift solutions which fit the observations. As suggested above, deeper ACS observations (an increase in sensitivity by a factor of 5 for the *F850LP* ACS filter) would make it possible to more confidently exclude many of the low redshift solutions.

## 4. DISCUSSION

The low S/N and large errors associated with the ACS, WFC3, and *Spitzer* observations of some of the faintest sources in the HUDF requires a more robust analysis than common  $\chi^2$  minimization techniques can provide. MCMC is able to provide this and allows us to derive accurate credible regions for redshifts, especially in the faint target, highest redshift regime. A complete SED analysis of the high redshift candidates discussed in this paper

shows that there is a significant possibility ( $\sim 1$  in 5) that these sources are low to moderate redshift ( $z < 4$ ) interlopers. This is in contrast to the results presented by Ellis et al. (2013), where they conclude that 7 out of 13 sources can be confidently classified as high- $z$  galaxies. Examining our 68% redshift credible regions might give the impression that our results agree well with those of Ellis et al. (2013). However, the limited number of measurements as well as the low S/N of the available measurements cause the redshift PDF of these sources to be highly non Gaussian. This in turn leads us to revise upward the probability that these sources are low redshift interlopers. In the end, we find that only the redshifts of the brightest y-dropouts in this sample are likely to be at a high redshift ( $z \approx 8$ ). Although the 128 orbits of the UDF12 have added considerable photometric depth to the UDF, the sources listed in Table 1 are still extremely faint. Moreover, given the large uncertainties in both flux and position, current IRAC observations do not strongly constrain the redshift of the vast majority of these objects. Similarly, the ACS observations are of insufficient depth to strongly constrain the SED blue-ward of the (presumptive) Lyman (or possibly Balmer) break.

Spectroscopic observations, while difficult and time consuming, still remain a viable method for further constraining the proposed photometric redshifts and have been attempted for two of the sources in Table 3. The first, UDF12-3954-6284, was observed using the WFC3 G141 grism ( $\lambda = 1.075\text{--}1.7 \mu\text{m}$  with  $\delta\lambda = 0.00465 \mu\text{m}$ ) as part of the 3D-HST survey (GO-12177; PI: van Dokkum) for two visits (4.7 ks each, the same orientation for each visit) and as a part of the CANDELS supernova follow-up program (GO-12099; PI: Riess) also for two visits (6.6 ks and 15 ks) each with a different orientation. Brammer et al. (2013) report a  $2.7\sigma$  detection of an emission line at  $1.599\mu\text{m}$  based on smoothing and cross correlating the 2D spectrum with a kernel constructed from the central  $0''.3$  of the *F160W* thumbnail image of UDF12-3954-6284 and removing any contamination using a contamination model (see their Figure 2). The object is not detected in any single visit. If the emission line were from  $\text{Ly}\alpha$  it would place the galaxy at  $z \sim 12$ , but Brammer et al. (2013) reject this possibility based not on the rest-frame equivalent width ( $\sim 170 \text{ \AA}$ ) but because  $\text{Ly}\alpha$  emission should be attenuated early in the epoch of re-ionization. Instead, they conclude the line is most likely [OIII], placing the object at  $z \sim 2.2$ . Ironically, UDF12-3954-6284 was detected in only one WFC3 broad band filter and is one of the three objects with the strongest probabilities of being at high redshift.

The second object with follow-up spectroscopic observations is UDFy-38135539, all of which were obtained with ground-based instruments. It was first observed with SINFONI on the VLT (integration time of 14.8 hr), centered on the *J*-band ( $1.1\text{--}1.4 \mu\text{m}$ ) resulting in a reported  $6\sigma$  detection of  $\text{Ly}\alpha$ , placing the galaxy at  $z = 8.555$  (Lehnert et al. 2010). Subsequent observations using X-SHOOTER ( $0.3\text{--}2.5 \mu\text{m}$ ) on the VLT and MOIRCS ( $0.9\text{--}1.78 \mu\text{m}$ ) on Subaru (5 hr and 11 hr integration times, respectively), have disputed this claim

based on non-detections of  $\text{Ly}\alpha$  (Bunker et al. 2013). They further noted that the  $F105W$  WFC3 photometry is inconsistent with both the line flux claimed by Lehnert et al. (2010) and the redshift from McLure et al. (2009). If the redshift were correct, then the  $F105W$  flux should be detected at  $15\sigma$ . The discrepancy between predicted  $F105W$  fluxes from SED-fitting (assuming high- $z$  and a real line detection) and the actual measured  $F105W$  fluxes raises some concern regarding the true nature of this object.

Using  $\pi\text{MC}^2$  we find that there are two populations of low- $z$  galaxies which fit the available data as well as the high- $z$  solutions. The first are low-moderate dusty systems at  $z \sim 2$ , the second are significantly dustier objects (up to  $A_V = 4$ ) at  $z < 1$ . Distinguishing between these low- $z$  solutions requires significantly more sensitive/deeper ACS and IRAC observations (see Figure 1) than are currently available (note: these would also serve to reject or improve the likelihood of high- $z$  redshifts as well). Deeper IRAC observations, should any be undertaken in the remaining time of the *Spitzer* Warm Mission, must contend with reaching source confusion limits as well as the higher background noise from operating in “warm mode.” Contrary to common wisdom and the conclusions reached by other high- $z$  studies, deeper observations blue-ward (e.g.  $F850LP$  or  $F814W$ ) of the presumptive break *would* be extremely useful. (see Figure 1). Alternatively, one can seek sources that are brightened by lensing due to foreground galaxy clusters to get more flux from high- $z$  sources (e.g. Coe et al. 2013). However, only a limited volume can be probed using this method.

Unfortunately, deeper observations in the optical bands using ACS are not likely considering the prohibitive observing times that would be required. Slitless spectroscopic observations using WFC3 with the G141 grism would provide an excellent method of rejecting or supporting the claims of high redshifts. However, this requires multiple position angles to avoid contamination from other objects or observational artifacts in the field as well as observations significantly deeper than those attempted to date (Pirzkal et al. 2012b). The G141 WFC3 grism observations would have the sensitivity to detect the emission lines potentially responsible for the observed photometric breaks. For example, in the case of object UDF12-3954-6284, an emission line with a flux as low as  $\approx 1.5 \times 10^{-18} \text{ erg s}^{-1} \text{ \AA}^{-1} \text{ cm}^{-2}$  could be solely responsible for a 29.3 mag detection in the  $F160W$  filter. Such a faint line would require upward of forty-two orbits to be *significantly* detected. In the absence of deeper HST or IRAC observations, observers will have to await the launch of *JWST*. We estimate that 10ks observations at  $0.9\mu\text{m}$  using NIRCAM with the *JWST* would be deep enough to confirm that the observed photometric breaks are strong enough to be 1216Å breaks. Until such observations are made, the nature as well as the volume density of very high redshift candidates are likely to remain uncertain unless significantly deeper ACS or WFC3 observations are taken. At the very least, our analysis suggests that the uncertainties

of current estimates of the volume density of these objects should be adjusted to account for the possibility that nearly one in four of these objects is not a high redshift galaxy.

Table 1.

Object	z	log(Mass) ( $M_{\odot}$ )	$A_V$	$f_{\text{esc}}$	log(Age) (Gyr)	$p^a$ (Min,Max)	$P(z < 4)^b$ (Min,Max)
UDF12-3895-7114	$8.5^{+2.3,+1.4}_{-2.2,-8.5}$	$7.6^{+0.8,+1.9}_{-0.9,-1.8}$	$0.8^{+0.7,+5.4}_{-0.8,-0.8}$	$0.5^{+0.2,+0.5}_{-0.5,-0.5}$	$-2.3^{+0.7,+2.5}_{-1.7,-1.7}$	0.11,0.23	0.30,0.40
UDF12-3921-6322	$8.8^{+0.9,+0.9}_{-0.5,-8.7}$	$7.5^{+0.7,+1.8}_{-0.6,-1.2}$	$0.5^{+0.5,+5.3}_{-0.5,-0.5}$	$0.5^{+0.2,+0.5}_{-0.5,-0.5}$	$-2.6^{+0.7,+2.6}_{-1.4,-1.4}$	0.01,0.05	0.06,0.21
UDF12-3947-8076 <sup>c</sup>	$8.6^{+0.8,+1.6}_{-0.4,-7.9}$	$8.1^{+0.6,+1.1}_{-0.6,-1.1}$	$0.6^{+0.3,+3.4}_{-0.6,-0.6}$	$0.6^{+0.4,+0.4}_{-0.2,-0.5}$	$-2.3^{+0.5,+2.3}_{-1.7,-1.7}$	0.01,0.31	0.03,0.84
UDF12-3954-6284 <sup>d</sup>	$12.0^{+0.3,+0.6}_{-0.3,-1.4}$	$7.8^{+0.4,+1.4}_{-0.5,-0.7}$	$0.0^{+0.2,+1.0}_{-0.0,-0.0}$	$0.5^{+0.2,+0.5}_{-0.5,-0.5}$	$-2.9^{+0.5,+1.6}_{-1.1,-1.1}$	0.00,0.24	0.00,0.13
UDF12-4106-7304	$9.4^{+2.1,+1.7}_{-1.2,-9.4}$	$7.7^{+0.8,+1.8}_{-0.9,-1.8}$	$0.7^{+0.7,+5.8}_{-0.7,-0.7}$	$0.5^{+0.5,+0.5}_{-0.2,-0.5}$	$-2.4^{+0.7,+2.6}_{-1.6,-1.6}$	0.06,0.35	0.12,0.28
UDF12-4265-7049	$9.1^{+1.3,+1.5}_{-0.9,-9.1}$	$7.8^{+0.7,+1.9}_{-0.9,-1.5}$	$0.6^{+0.6,+5.2}_{-0.6,-0.6}$	$0.5^{+0.2,+0.5}_{-0.5,-0.5}$	$-2.4^{+0.6,+2.4}_{-1.6,-1.6}$	0.06,0.19	0.18,0.26
UDF12-4344-6547	$8.7^{+0.9,+1.1}_{-0.6,-8.5}$	$7.5^{+0.7,+1.9}_{-0.8,-1.2}$	$0.5^{+0.5,+4.8}_{-0.5,-0.5}$	$0.5^{+0.2,+0.5}_{-0.5,-0.5}$	$-2.6^{+0.6,+2.3}_{-1.4,-1.4}$	0.03,0.13	0.14,0.23
UDFj-35427336	$3.4^{+5.5,+6.6}_{-3.4,-3.4}$	$7.7^{+1.1,+1.3}_{-0.8,-2.6}$	$1.7^{+1.9,+6.0}_{-1.7,-1.7}$	$0.5^{+0.2,+0.5}_{-0.5,-0.5}$	$-2.0^{+0.8,+2.5}_{-2.0,-2.0}$	0.16,0.47	0.40,0.50
UDFj-38116243	$9.6^{+2.4,+1.9}_{-1.3,-9.6}$	$7.8^{+0.8,+2.0}_{-1.0,-1.8}$	$0.9^{+0.7,+5.7}_{-0.9,-0.9}$	$0.5^{+0.2,+0.5}_{-0.5,-0.5}$	$-2.3^{+0.7,+2.4}_{-1.7,-1.7}$	0.13,0.50	0.20,0.30
UDFj-43696407	$2.1^{+6.7,+9.0}_{-2.1,-2.1}$	$7.5^{+1.2,+1.9}_{-0.7,-2.5}$	$2.0^{+1.8,+5.4}_{-2.0,-2.0}$	$0.5^{+0.2,+0.5}_{-0.5,-0.5}$	$-2.0^{+0.9,+2.5}_{-2.0,-2.0}$	0.78,1.00	0.41,0.92
UDFy-33436598	$7.8^{+0.7,+0.9}_{-0.4,-7.3}$	$7.7^{+0.4,+1.3}_{-0.3,-0.9}$	$0.6^{+0.3,+2.9}_{-0.6,-0.6}$	$0.5^{+0.5,+0.5}_{-0.2,-0.4}$	$-2.6^{+0.6,+2.5}_{-1.4,-1.4}$	0.01,0.05	0.09,0.32
UDFy-37796000 <sup>e</sup>	$8.1^{+0.2,+0.5}_{-0.2,-6.6}$	$7.7^{+0.3,+0.8}_{-0.4,-0.6}$	$0.3^{+0.2,+2.7}_{-0.3,-0.3}$	$0.6^{+0.4,+0.4}_{-0.2,-0.5}$	$-2.9^{+0.4,+1.3}_{-1.1,-1.1}$	0.00,0.00	0.00,0.08
UDFy-38135539 <sup>c</sup>	$8.4^{+0.2,+0.3}_{-0.2,-0.3}$	$8.1^{+0.4,+0.8}_{-0.5,-0.7}$	$0.5^{+0.2,+0.8}_{-0.5,-0.5}$	$0.7^{+0.3,+0.3}_{-0.2,-0.6}$	$-2.6^{+0.4,+1.1}_{-1.4,-1.4}$	0.00,0.69	0.00,0.13
Average							0.21

Table 3. Derived physical properties of  $z > 8$  candidates in the HUDF

Note. — This table lists the median values for each parameter as well as the 68% and 95% credible regions (highest posterior density regions), separated by a comma, when using BC03 stellar population models.

a - Likelihood ratio test significance when comparing the quality of the best fitting model to the quality of the best fit at  $z < 4$ . Significance values greater than 0.05 ( $2\sigma$ ) imply that high redshift models do not fit the data significantly better. The minimum and maximum values of  $p$  across all seven different input models are shown.

b - Probability that this object is at  $z < 4$ . The minimum and maximum values of  $P(z < 4)$  across all seven different input models are shown.

c - MA05 models without nebular emission reject all low  $z$  solutions for this object.

d - BC03 models with exponentially decaying SFH and CB07 models do not reject low redshift solutions.

The nature of this object is further discussed in Section 3.  
e - CB07 and MA05 models lead to the rejection of low redshift solutions.

## 5. Acknowledgment

We would like to warmly thank J. M. Miralles for a fruitful discussion of the working of `hyperz`. We would also like to thank F. Pierfederici for his contributions that ultimately allowed us to run  $\pi\text{MC}^2$  on distributed computers using Celery and HT-Condor. Finally, we thank Dr. Richard Ellis, Dr. Ross McLure and Dr. Rychard Bouwens and their collaborators for constructive and insightful comments.

## REFERENCES

- Atek, H., Siana, B., Scarlata, C., et al. 2011, *ApJ*, 743, 121
- Bolzonella, M., Miralles, J.-M., & Pelló, R. 2000, *A&A*, 363, 476
- Bouwens, R. J., Illingworth, G. D., Labbe, I., et al. 2011, *Nature*, 469, 504
- Brammer, G. B., van Dokkum, P. G., Illingworth, G. D., et al. 2013, *ApJL*, 765, L2
- Bremer, M. N., Jensen, J. B., Lehnert, M. D., et al. 2004, *ApJL*, 615, L1
- Bruzual, G., & Charlot, S. 2003, *MNRAS*, 344, 1000
- Bunker, A. J., Caruana, J., Wilkins, S. M., et al. 2013, *MNRAS*, 430, 3314
- Capak, P., Mobasher, B., Scoville, N. Z., et al. 2011, *ApJ*, 730, 68
- Charlot, S., Bruzual, G., 2013, in prep
- Chary, R. R., Teplitz, H. I., Dickinson, M. E. et al. 2007, *ApJ*, 665, 257
- Coe, D., Zitrin, A., Carrasco, M., et al. 2013, *ApJ*, 762, 32
- Dickinson, M., Stern, D., Giavalisco, H. C. et al. 2004, *ApJL*, 600, 99
- Ellis, R. S., McLure, R. J., Dunlop, J. S., et al. 2013, *ApJL*, 763, L7
- Fan, X., Strauss, M. A., Becker, R. H., et al. 2006, *AJ*, 132, 117
- Henry, A. L., Malkan, M. A., Colbert, J. W., et al. 2008, *ApJL*, 680, L97
- Henry, A. L., Siana, B., Malkan, M. A. et al. 2009, *ApJ*, 697, 1128
- Hu, E. M., Cowie, L. L., Capak, P. et al. 2004, *AJ*, 127, 563



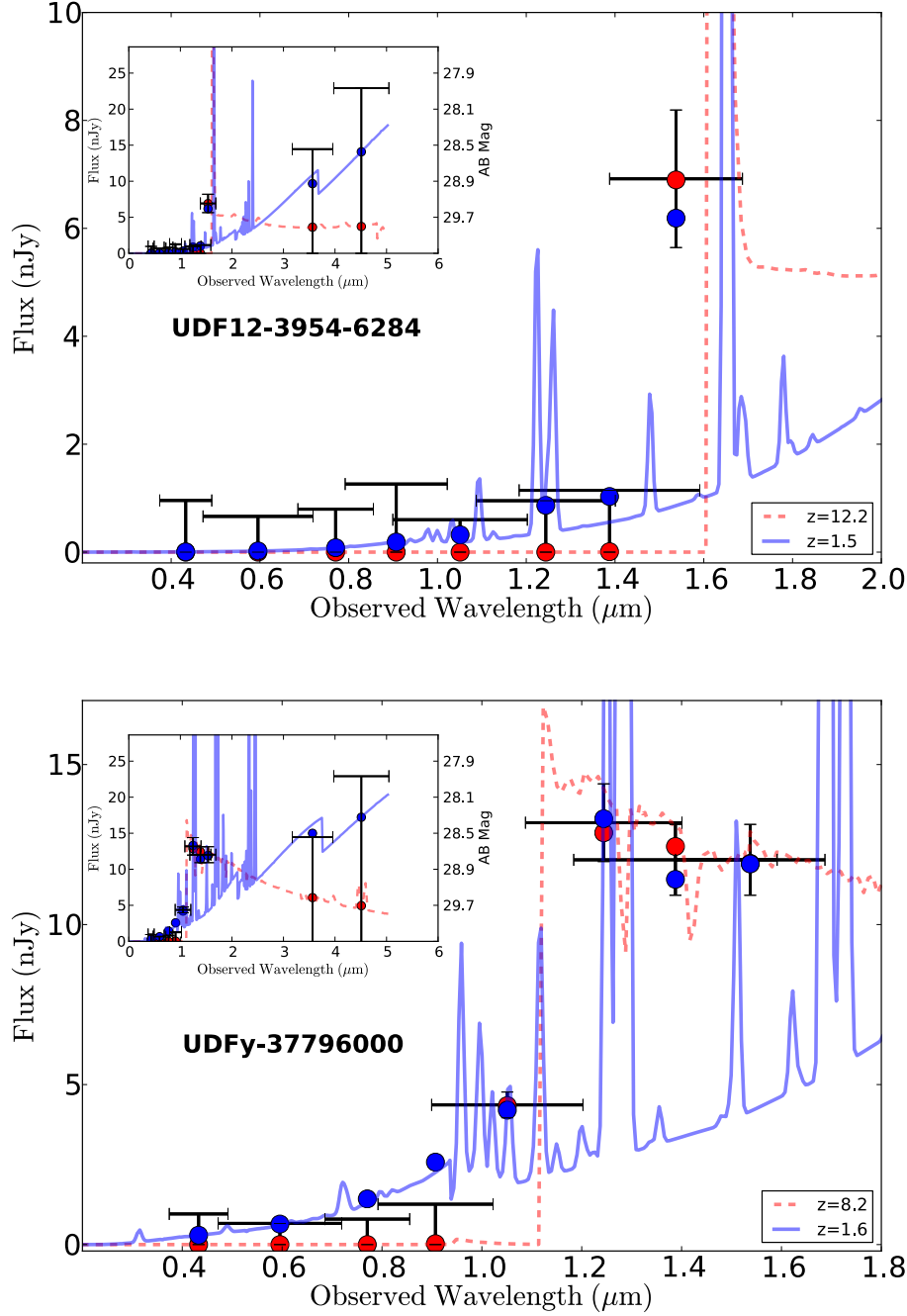


Fig. 1.— High and low redshift solutions to the observed photometry of objects UDF12-3954-6284 and UDFy-37796000. The upper left sub-panels show all of the available photometry, including the infrared IRAC upper limits. The main panels show the observed UV to NIR (ACS and WFC3 bands) region for the same object. Two models are shown in each case. The first, shown in a dashed red line, is a  $z > 8$  model while the solid blue line shows a much lower redshift solution at  $z \approx 2$ . Observed fluxes are shown using error bars. Synthetic model fluxes in each observed filter are shown using large circles.

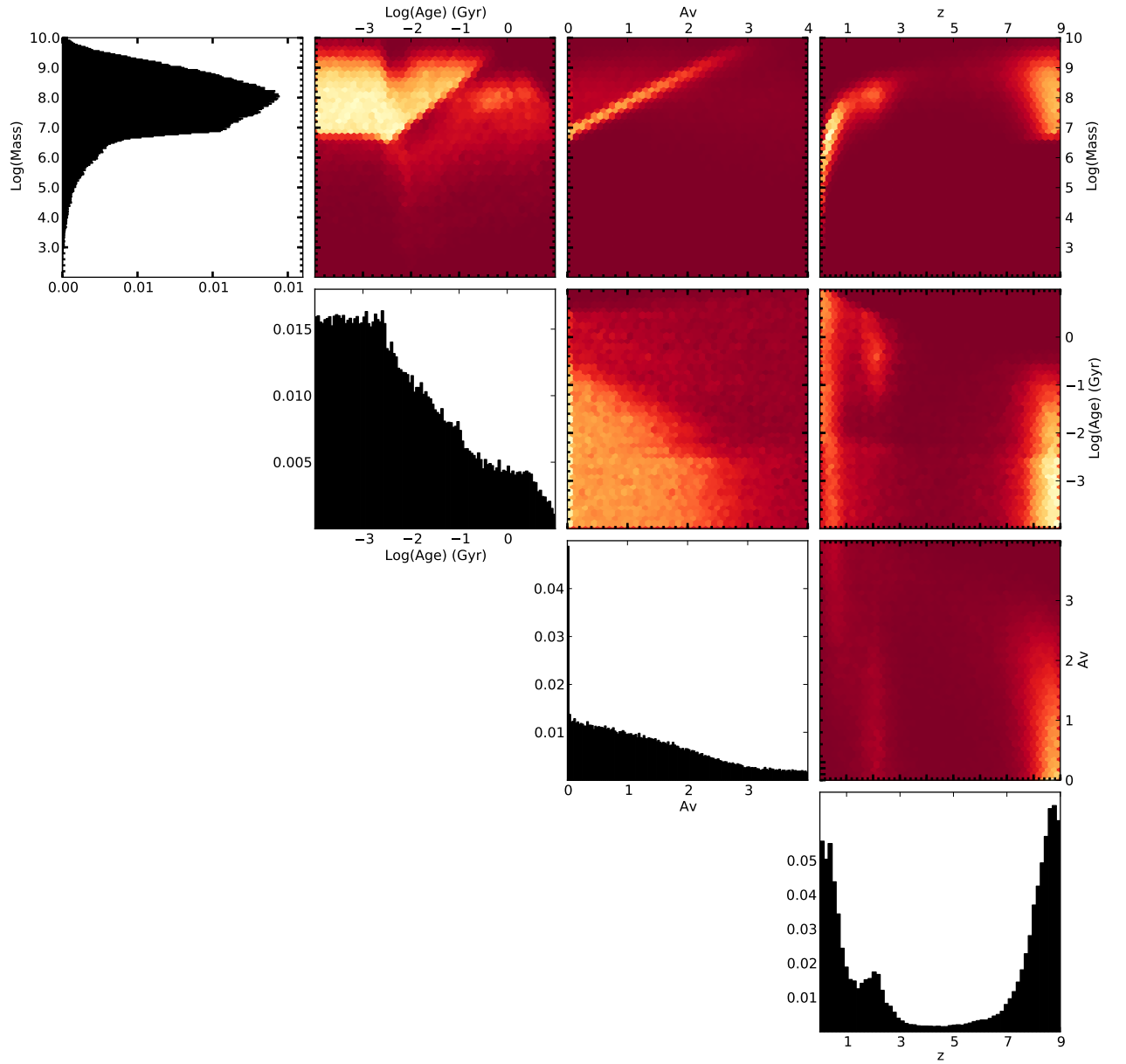


Fig. 2.— Posterior probability density function estimates for object UDF12-3895-7114. The non-Gaussian, multi-modal nature of the redshift distribution is evident in the rightmost plots.

- Komatsu, E., Smith, K. M., Dunkley, J., et al. 2011, *ApJS*, 192, 18
- Labbé, I, Franx, M., Rudnick, G. et al. 2003, *AJ*, 125, 1107
- Labbé, I, Gonzalez, V., Bouwens, R. J. et al. 2010, *ApJ*, 716, 103
- Lehnert, M. D., Förster-Schreiber, N. M., & Bremer, M. N. 2005, *ApJ*, 624, 80
- Lehnert, M. D., Nesvadba, N. P. H., Cuby, J. G., et al. 2010, *Nature*, 467, 940
- Malhotra, S., Rhoads, J., Dey, A., Stern, D., & Spinrad, H. 2001, in *ASP Conf. Proc.* 240, *Gas and Galaxy Evolution*, ed. J. E. Hibbard, M. Rupen, & J. H. van Gorkom (San Francisco, CA: ASP), 97
- Malhotra, S., Rhoads, J. E., Pirzkal, N., et al. 2005, *ApJ*, 626, 666
- Maraston, C. 2005, *MNRAS*, 362, 799
- McLure, R. J., Cirasuolo, M., Dunlop, J. S. et al. 2009, *MNRAS*, 395, 2196
- McLure, R. J., Dunlop, J. S., Cirasuolo, M., et al. 2010, *MNRAS*, 403, 960
- McLure, R. J., Dunlop, J. S., de Ravel, L., et al. 2011, *MNRAS*, 418, 2074
- Mobasher, B., Dickinson, M., Ferguson, H. C. et al. 2005, *ApJ*, 635, 832
- Papovich, C., Dickinson, M., Ferguson, H. C. et al. 2001, *ApJ*, 559, 620
- Papovich, C., Finkelstein, S. L., Ferguson, H. C., Lotz, J. M., & Giavalisco, M. 2011, *MNRAS*, 412, 1123
- Pelló, R., Schaerer, D., Richard, J., et al. 2004, *A&A*, 416, L35
- Pirzkal, N., Malhotra, S., Rhoads, J. E., & Xu, C. 2007, *ApJ*, 667, 49
- Pirzkal, N., Rothberg, B., Nilsson, K. K., et al. 2012, *ApJ*, 748, 122
- Pirzkal, N., Rothberg, B., Chun, L., et al. 2012, *ApJ*, accepted (arXiv:1208.5535)
- Pirzkal, N., Xu, C., Malhotra, S., et al. 2004, *ApJS*, 154, 501
- Richard, J., Kneib, J. P., Ebeling, H. et al. 2011, *MNRAS*, 414, L31
- Rhoads, J. E., Malhotra, S., Pirzkal, N., et al. 2009, *ApJ*, 697, 942
- Schaerer, D., & Pelló, R. 2005, *MNRAS*, 362, 1054

- Songaila, A., & Cowie, L. L. 2002, *AJ*, 123, 2183
- Stanway, E. R., Bremer, M. N., & Lehnert, M. D. 2008, *MNRAS*, 385, 493
- Thompson, R. I., Weymann, R. J., & Storrie-Lombardi, L. J. 2001, *ApJ*, 546, 694
- Weatherley, S. J., Warren, S. J., & Babbedge, T. S. R. 2004, *A&A*, 428, L29
- Yan, H.-J., Windhorst, R. A., Hathi, N. P., et al. 2010, *RAA*, 10, 867